

Removing the deadwood from DFT/MRCI wave functions: The p-DFT/MRCI method

Simon P. Neville^{*,†} and Michael S. Schuurman^{*,†,‡}

[†]*National Research Council of Canada, 100 Sussex Drive, Ottawa, Ontario K1A 0R6, Canada*

[‡]*Department of Chemistry and Biomolecular Sciences, University of Ottawa, 10 Marie Curie, Ottawa, Ontario, K1N 6N5, Canada*

E-mail: Simon.Neville@nrc-cnrc.gc.ca; Michael.Schuurman@nrc-cnrc.gc.ca

Abstract

The combined density functional theory and multireference configuration interaction (DFT/MRCI) method is a powerful tool for the calculation of excited electronic states of large molecules. There exists, however, a large amount of superfluous configurations in a typical DFT/MRCI wave function. We show that this deadwood may be effectively removed using a simple configuration pruning algorithm based on second-order Epstein-Nesbet perturbation theory. The resulting method, which we denote p-DFT/MRCI, is shown to result in orders of magnitude saving in computational timings, while retaining the accuracy of the original DFT/MRCI method.

1 Introduction

Since its introduction by Grimme and Waletzke,¹ the combined density functional theory and multireference configuration interaction (DFT/MRCI) method has proved to be a uniquely

powerful tool for the calculation of the excited states of large molecular systems. The method was originally conceived as a means to calculate singlet and triplet valence excited states of organic molecules. However, the scope of the method has recently been significantly widened to include multiplicity-independent formulations,^{2,3} a parameterization tuned to the description of transition metal complexes,⁴ the treatment of core-excited states,⁵ and the calculation of spin-orbit and non-adiabatic couplings^{6,7} and diabatic potentials.⁸

At its heart, DFT/MRCI is an individually selecting MRCI method, utilizing short MRCI expansions to describe static electronic correlation and DFT-specific Hamiltonian matrix corrections to capture the remaining dynamic correlation.⁹ As a result, DFT/MRCI wave function expansions are extremely compact relative to those in canonical MRCI methods. Experience has shown, however, that DFT/MRCI wave functions typically contain a large amount ($\gtrsim 90\%$) of deadwood configurations. That is, configurations that contribute negligibly to the norm of a DFT/MRCI wave function. If these configurations could be identified *a priori* and removed, then large computational savings would be afforded.

The study of algorithms for the removal of superfluous configurations from CI calculations dates back to the earliest days of the field with the pioneering work of Davidson¹⁰ and Whitten and Hackmeyer.^{11,12} Other notable early examples include the multi-reference double-excitation CI (MRD-CI) method of Buenker and Peyerimhoff¹³⁻¹⁵ and the CI by perturbation with multiconfigurational zeroth-order wavefunction selected by iterative process (CIPSI) method of Huron *et al.*¹⁶ Recent years have seen a resurgence of interest in such selected CI methods. Prominent examples include the refinement of the CIPSI methodology by Scemama and co-workers,¹⁷⁻¹⁹ the semistochastic heat-bath CI (SHCI),²⁰⁻²³ adaptive sampling CI (ASCI),^{24,25} adaptive CI (ACI),^{26,27} iterative CI (iCI),^{28,29} and iterative configuration expansion (ICE)^{30,31} methods. Common to many of the above mentioned selected CI methods is the use of aspects of second-order Epstein-Nesbet perturbation theory (ENPT2) to estimate the importance of individual determinants or configuration state functions (CSFs) via their interaction with a set of zeroth-order eigenfunctions.

The use of ENPT2 to estimate *a priori* the importance of individual configurations is readily applicable within the framework of the DFT/MRCI method, and it is the purpose of this paper to explore this as a route to the elimination of the deadwood from DFT/MRCI wave functions. As we shall detail, for large molecules, it is found possible to reduce the size of the DFT/MRCI configuration space by orders of magnitude. By applying a perturbative energy correction to account for the discarded configurations, the errors in the computed excitation energies can be made essentially negligible (~ 1 meV). We denote the combined application of configuration pruning and perturbative energy corrections to DFT/MRCI wave functions as p-DFT/MRCI.

The rest of the paper is arranged as follows. In Section 2, we give a brief overview of the DFT/MRCI method, focusing on the aspects pertinent to the problem of the removal of deadwood configurations. Section 3 gives the algorithmic details of the p-DFT/MRCI method. In Section 4, we present an analysis of the errors of the excitation energies furnished by p-DFT/MRCI relative to the original DFT/MRCI method. In Section 4.4, we give an analysis of the computational costs of the p-DFT/MRCI method. Finally, in Section 5, we provide our concluding remarks on the utility of the proposed methodology and the new research avenues opened by it.

2 The DFT/MRCI method

The electronic Hamiltonian is represented in the DFT/MRCI method in a basis of CSFs $|\mathbf{w}\omega\rangle$ built from canonical Kohn-Sham (KS) orbitals. Here, \mathbf{w} denotes a spatial occupation and ω a spin-coupling pattern pertaining to the open shells in \mathbf{w} . The total set of CSFs $\Omega = \{|\mathbf{w}\omega\rangle\}$ is obtained from the set of single and double excitations from a small reference space $\Omega_0 = \{|\mathbf{w}_0\omega\rangle\}$, where the \mathbf{w}_0 denote the reference space configurations. In the following we will refer to $\Omega_F = \Omega \setminus \Omega_0$ as the first-order interacting space (FOIS).

The on-diagonal elements of the DFT/MRCI Hamiltonian matrix take the form of the

sum of the exact result and DFT-specific corrections:

$$\left\langle \text{w}\omega \left| \hat{H}^{DFT} - E_{DFT} \right| \text{w}\omega \right\rangle = \left\langle \text{w}\omega \left| \hat{H} - E_{SCF} \right| \text{w}\omega \right\rangle + \sum_p \Delta w_p (\epsilon_p^{KS} - F_{pp}) + \Delta E_x + \Delta E_c. \quad (1)$$

Here, $\Delta w_p = w_p - \bar{w}_p$ denotes the difference of the occupation of the p th spatial orbital relative to a base, or anchor, occupation \bar{w} , chosen as the Hartree-Fock occupation. ϵ_p^{KS} and F_{pp} denote, respectively, the KS orbital energies and on-diagonal elements of the Fock operator in the KS orbital basis. Finally, ΔE_x and ΔE_c are Coulomb and exchange corrections, the exact form of which varies with the different DFT/MRCI parameterizations.¹⁻⁴

The role played by the DFT-specific corrections in Equation 1 is to account for the dynamic electron correlation that would otherwise be described by the coupling between different CSFs in the MRCI expansion. Thus, the off-diagonal Hamiltonian matrix elements in question must also be modified to avoid a double counting of dynamic correlation. This is achieved by introducing a damping of the off-diagonal elements that is dependent on the energetic separation of the bra and ket CSFs:

$$\left\langle \text{w}\omega \left| \hat{H}^{DFT} - E_{DFT} \right| \text{w}'\omega' \right\rangle = \left\langle \text{w}\omega \left| \hat{H} - E_{SCF} \right| \text{w}'\omega' \right\rangle \cdot D(\Delta E_{\text{w}\omega\text{w}'\omega'}), \quad (2)$$

where

$$\Delta E_{\text{w}\omega\text{w}'\omega'} = \frac{1}{n_\omega} \sum_\omega^{n_\omega} H_{\text{w}\omega, \text{w}\omega}^{DFT} - \frac{1}{n_{\omega'}} \sum_{\omega'}^{n_{\omega'}} H_{\text{w}'\omega', \text{w}'\omega'}^{DFT} \quad (3)$$

denotes the spin coupling-averaged difference between the on-diagonal matrix elements corresponding to the spatial occupations w and w' . $D(\Delta E)$ is a some rapidly decaying function, chosen in practice to be an exponential^{1,4} or inverse arctangent function.^{2,3}

The effect of damping the off-diagonal Hamiltonian matrix elements is to decouple CSFs that are energetically well separated. As well as minimizing the double counting of dynamic

correlation, this also means that CSFs of the reference space, Ω_0 , become decoupled from the vast majority of the CSFs spanning the FOIS, Ω_F . This leads to one of the most important aspects of the DFT/MRCI methodology: the ability to discard almost all of the FOIS CSFs. In practice, this is achieved using the following simple energy-based selection criterion. For each FOIS configuration w , the quantity

$$d_w = \sum_p \Delta_{w_p} \epsilon_p^{KS} - \delta E_{sel} \quad (4)$$

is computed, where the parameter δE_{sel} is conventionally chosen as either 0.8 or 1.0 E_h .¹ If d_w is less than the highest reference space eigenvalue of interest, then all the CSFs generated from the configuration w are selected for inclusion, else they are discarded.

3 The pruned DFT/MRCI method: p-DFT/MRCI

3.1 Deadwood in the DFT/MRCI CSF space

The result of the energy-based selection criterion is a reduction of the number of CSFs by many orders of magnitude. However, it is found that a large amount of deadwood CSFs are still present when this is the sole selection criterion used. By a deadwood CSF we here mean one that contributes negligibly to the eigenfunctions of interest.

By way of illustration, consider the projection of a given DFT/MRCI eigenfunction $|\psi_I\rangle$ onto the space spanned by the first N CSFs importance ordered by their absolute coefficient values:

$$|\tilde{\psi}_I^{(N)}\rangle = \sum_{w\omega}^N |w\omega\rangle \langle w\omega|\psi_I\rangle = \hat{P}_N |\psi_I\rangle. \quad (5)$$

By plotting the norm of $\hat{P}_N |\psi_I\rangle$ as a function of N , we may visualize the amount of deadwood present in the eigenfunction $|\psi_I\rangle$. This is shown in Figure 1 for a DFT/MRCI calculation of the first five excited states of butadiene computed using the aug-cc-pVDZ basis.

It is clear that with a couple of hundred CSFs, near unit norms of all five eigenfunctions are attained. This is only a small fraction of the total of 41681 CSFs that result from the energy-based selection criterion. Considering that the computational effort of a DFT/MRCI Hamiltonian build with the number of CSFs has a scaling of $\mathcal{O}(N^m)$, $m \sim 1.3 - 1.5$, we see that significant computational savings could be realized if the deadwood CSFs could be identified and removed.

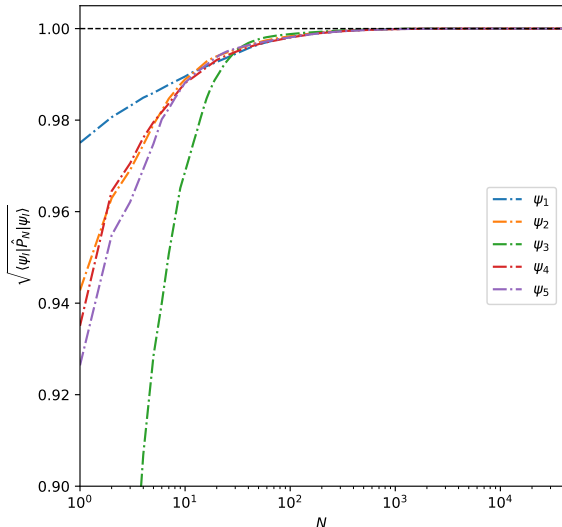


Figure 1: Measure of the “deadwood” in DFT/MRCI wave functions: the norms of the first five excited state DFT/MRCI/aug-cc-pVDZ eigenfunctions of butadiene projected onto the first N highest weight CSFs. Wave function norms greater 0.999 are achieved with fewer than 200 CSFs per state.

3.2 Configuration pruning

Assume that a reference space diagonalization has been performed, furnishing reference space eigenpairs $|\psi_I^{(0)}\rangle$ and $E_I^{(0)}$, and that the usual energy-based selection criterion has been used to construct a set Ω of CSFs. Our aim is to apply a further pruning of the set Ω , removing those FOIS CSFs that will not contribute significantly to the final DFT/MRCI eigenfunctions. To do so, we estimate the contribution to each FOIS CSF to the final DFT/MRCI eigenfunctions

using ENPT2.

In ENPT2, the full CSF space is partitioned into two subspaces, termed the P and Q spaces. The zeroth-order Hamiltonian, \hat{H}_0 , is taken to be block diagonal between the P and Q spaces and diagonal within the Q space. That is

$$\hat{H}_0 = \sum_{w\omega \in P} \sum_{w'\omega' \in P} |w\omega\rangle \langle w\omega| \hat{H}^{DFT} |w'\omega'\rangle \langle w'\omega'| + \sum_{w\omega \in Q} |w\omega\rangle \langle w\omega| \hat{H}^{DFT} |w\omega\rangle \langle w\omega|, \quad (6)$$

Within the context of a DFT/MRCI calculation, the natural choice is to identify the P space with the reference CSFs, and the Q space with the FOIS CSFs that have survived the energy-based selection criterion. Then, the ENPT2 approximations to the DFT/MRCI wave functions read

$$|\psi_I\rangle \approx |\psi_I^{(0)}\rangle + |\psi_I^{(1)}\rangle, \quad (7)$$

with

$$|\psi_I^{(1)}\rangle = \sum_{w\omega \notin \Omega_0} A_{w\omega}^{(I)} |w\omega\rangle, \quad (8)$$

$$A_{w\omega}^{(I)} = \frac{\langle w\omega | \hat{H}^{DFT} | \psi_I^{(0)} \rangle}{E_I^{(0)} - \langle w\omega | \hat{H}^{DFT} - E_{DFT} | w\omega \rangle}. \quad (9)$$

The absolute values of the coefficients $A_{w\omega}^{(I)}$ give a measure of the importance of the FOIS CSF $w\omega$ to the I th DFT/MRCI eigenfunction. Importantly, these may be determined with minimal computational cost using the reference space eigenpairs and the FOIS CSFs that have passed the energy-based selection criterion.

As DFT/MRCI is most efficiently implemented as a configuration-driven method, in practice we discard those configurations that do not generate any CSFs contributing significantly

to the ENPT2 first-order wave function corrections. Our implementation is as follows. The vectors $\mathbf{A}^{(I)}$ of ENPT2 first-order corrections are computed for all reference space states $|\psi_I^{(0)}\rangle$. For each state, the smallest subset S_I of FOIS configurations satisfying

$$\sum_{w \in S_I} \sum_{\omega} |A_{w\omega}^{(I)}|^2 \geq \alpha_p |\mathbf{A}^{(I)}|^2 \quad (10)$$

are determined, where $\alpha_p < 1$. The final subset of FOIS configurations chosen for inclusion in the p-DFT/MRCI calculation is then taken as the union of the subsets S_I for each state. As the vast majority of FOIS configurations have already been removed by the energy-based selection criterion, this additional pruning step is extremely cheap. Furthermore, the accuracy of the p-DFT/MRCI eigenpairs (relative to the unpruned ones) is systematically controlled by the single parameter α_p .

It remains to note that, in practice, if the n lowest energy DFT/MRCI states are required, they will not generally correspond to the first n reference space states. As such, we include a small number $n_{extra} \approx 10$ of extra reference space states, and pick the n roots with the lowest ENPT2-corrected energies for use in the configuration pruning.

3.3 ENPT2 energy corrections

The configuration pruning algorithm presented in Section 3.2 is controlled by the pruning threshold α_p that enters into Equation 10. The smaller the value of α_p , the greater the proportion of FOIS CSFs are discarded, but to the increasing detriment of the resulting p-DFT/MRCI energies. In order to use as small a pruning threshold as possible, the contributions of the discarded CSFs to the DFT/MRCI energies can be accounted for perturbatively. To do so, the ENPT2 energy corrections

$$E_{I,w\omega}^{(2)} = \frac{\left| \langle w\omega | \hat{H}^{DFT} | \psi_I^{(0)} \rangle \right|^2}{E_I^{(0)} - \langle w\omega | \hat{H}^{DFT} - E_{DFT} | w\omega \rangle} \quad (11)$$

are computed for the discarded CSFs. These corrections are then added to the energies computed using the pruned CSF basis. In practice, this allows for a significantly greater proportion of FOIS CSFs to be discarded while maintaining the accuracy of the resultant energies. Importantly, these energy corrections are essentially “free” with the evaluation of the first-order wave function corrections (Equation 9). From here on out, we will use the term p-DFT/MRCI to refer to the combination of configuration pruning *and* the application of the ENPT2 energy corrections (Equation 11).

3.4 Automated selection of the reference space

In a standard (unpruned) DFT/MRCI calculation the initial choice of reference space configurations is not particularly critical to the quality of the resulting DFT/MRCI wave functions. The reason for this is that a DFT/MRCI calculation is typically performed in the following iterative fashion. First, a guess reference space is selected, and the DFT/MRCI wave functions are computed using this initial space. Next, the reference space is updated to contain the dominant configurations present in the DFT/MRCI wave functions, and the calculation is repeated. This reference space refinement is continued until convergence of the DFT/MRCI wave functions is attained, a process usually requiring only a couple of iterations.

However, the use of Epstein-Nesbet perturbation theory in p-DFT/MRCI is predicated on the reference space states $|\psi_I^{(0)}\rangle$ being good zeroth-order descriptions of the states of interest. As such, the configuration pruning and ENPT2 energy correction algorithms can yield poor results if the initial reference space is not chosen reasonably. For large numbers of states, a good choice of the initial reference space may not be obvious, and it is desirable to automate its generation. In order to arrive at a robust, fully automated algorithm, we first note that, from experience, the use of a restricted active space CI (RASCI)³² set of configurations with only the RAS1 (characterized by a maximum number of holes) and RAS3 (defined by a maximum number of electrons) subspaces occupied is almost always a good choice for the initial reference space. The problem then shifts to the selection of the RAS1 and RAS3 MOs.

To automatically select the RAS1 and RAS3 MOs, we have explored the use of a computationally cheap, preliminary combined DFT and CIS (DFT/CIS) calculation,³³ selecting the particle/hole MOs that appear in the dominant DFT/CIS configurations. In practice we have found this to be a robust route to the generation of initial reference spaces that yield good quality zeroth-order wave functions. However, for large systems, this preliminary DFT/CIS calculation can become more expensive than the pruned DFT/MRCI calculation itself. To overcome this, an aggressively loose integral pre-screening is introduced into the DFT/CIS calculation, making use of the Cauchy-Schwarz inequality

$$|(pq|rs)| \leq \sqrt{(pq|pq)}\sqrt{(rs|rs)} = G_{pq}G_{rs}. \quad (12)$$

In evaluating the DFT/CIS equations, off-diagonal Hamiltonian matrix elements H_{mn} with bra and ket configurations corresponding to excitation from MOs $i \rightarrow a$ and $j \rightarrow b$ are skipped if

$$\frac{1}{2}G_{ij}G_{ab} < \tau \quad \text{and} \quad 2G_{ia}G_{jb} < \tau. \quad (13)$$

In practice, using a large integral screening threshold $\tau = \mathcal{O}(10^{-2})$ is found to furnish a rather severe, but uniform, degradation of the quality of the resulting DFT/CIS energies. As such, the particle/hole MOs of the dominant configurations may still be reliably identified, but at a much reduced cost.

3.5 Implementation and computational details

All p-DFT/MRCI calculations were performed using a newly developed software package tailored for the calculation of excited electronic states using CI with generalized reference spaces.³⁴ The required KS MOs, energies and integrals were computed using the PySCF package.^{35,36} The density fitting approximation³⁷⁻³⁹ was used in the evaluation of the two-electron integrals. Following the original DFT/MRCI implementation by Grimme and Walet-

zke,¹ ideas from the works of Segal *et al.*^{40,41} and Engels and Hanrath⁴² were used in the evaluation of the DFT/MRCI Hamiltonian matrix elements. Additionally, aspects of the bitstring-based algorithms of Scemama, Giner and Garniron were adapted for the computation of spin-coupling coefficients and the identification of non-zero Hamiltonian matrix elements in a CSF basis.^{19,43}

The automatic initial reference space generation algorithm described in Section 3.4 is based on a preliminary DFT/CIS calculation. The original DFT/CIS Hamiltonian was parameterised for use with the B3LYP functional.³³ However, all current DFT/MRCI implementations are parameterised for use with the BHLYP functional. Ideally, then, the parameters of the DFT/CIS would be reoptimized for use with the same functional, but this is somewhat beyond the scope of this preliminary work. As such, in a first step, the parameters of Grimme’s DFT/CIS Hamiltonian were used, with the Coulomb scaling parameter (c_1 in the notation of Reference 33) manually adjusted to yield acceptable excitation energies for a small number of molecules. In all calculations described here, a value of $c_1 = 0.596$ was used.

To assess the efficacy of the p-DFT/MRCI methodology, vertical excitation energies were computed for the molecules in Thiel’s test set of 28 small-to-medium sized organic molecules.⁴⁴ For each molecule, four singly excited states of each symmetry were computed, resulting in a total of 472 excitation energies, including those of both valence and Rydberg character. In all cases, the original DFT/MRCI Hamiltonian parameterization of Grimme and Waletzke¹ was used, although we expect the conclusions drawn to apply similarly to the re-designed Hamiltonians of Marian *et al.*²⁻⁴ All calculations were performed using the aug-cc-pVDZ basis⁴⁵ and aug-cc-pVDZ-jkfit auxiliary basis.

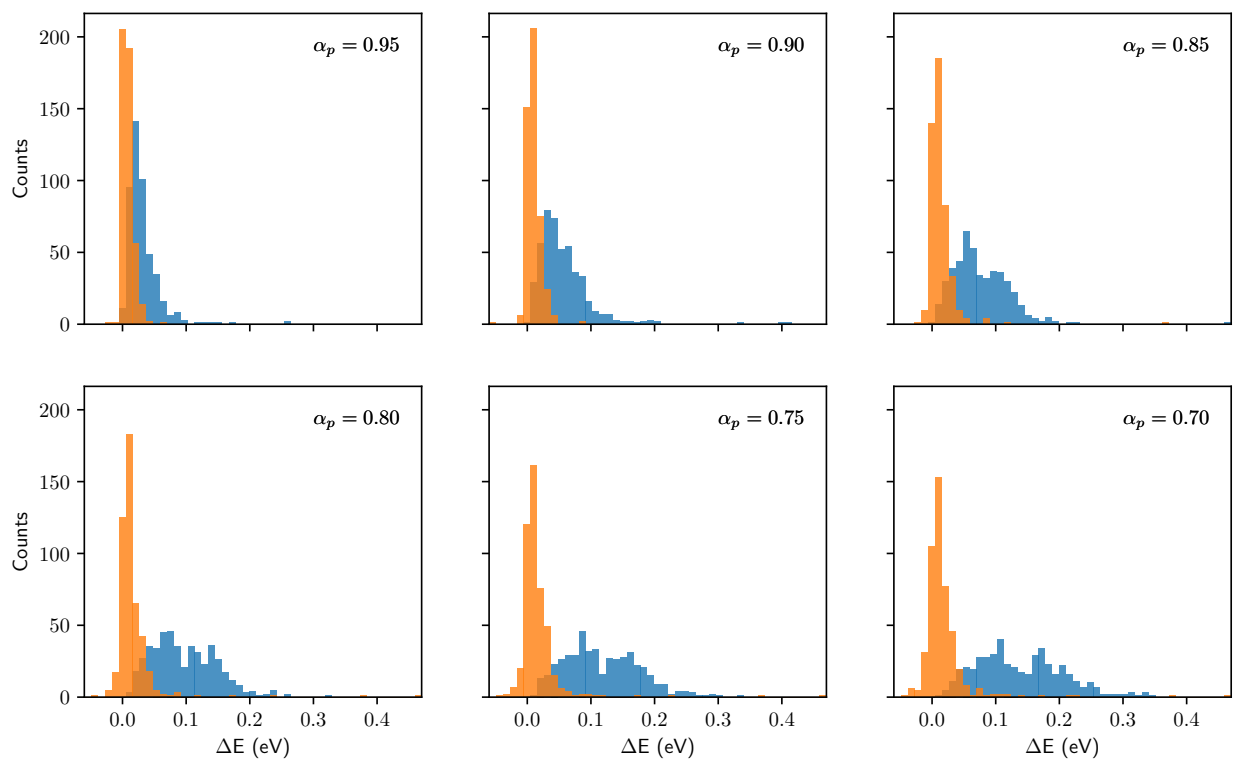


Figure 2: Excitation energy errors as a function of the pruning threshold α_p relative to the unpruned values. Orange: ENPT2 energy-corrected values. Blue: uncorrected values.

4 Results

4.1 Error analysis

We first consider the errors introduced as a function of the pruning threshold α_p . To do so, all 472 excitation energies in the test set were computed using a fixed energy-based selection threshold of $\delta E_{sel} = 1.0 E_h$ and α_p set to values between 1.0 (unpruned) and 0.70. Shown in Figure 2 are the differences, ΔE , in the computed excitation energies relative to the unpruned values as a function of α_p . For comparison, the differences ΔE for both the uncorrected (blue) and ENPT2 energy-corrected (orange) values are shown.

With the application of the ENPT2 energy correction, for the two tightest thresholds ($\alpha_p = 0.95$ and $\alpha_p = 0.90$), the errors introduced by the configuration pruning procedure are extremely small, with root mean square deviations (RMSDs) not exceeding 0.015 eV. Decreasing the value of α_p steadily increases the RMSD of the computed ENPT2-corrected excitation energies. However, even with the rather loose pruning threshold of $\alpha_p = 0.7$, an RMSD of only 0.041 eV is attained. At this level of pruning, FOIS CSFs that contribute non-negligibly to the DFT/MRCI wave functions are being discarded. However, the use of ENPT2 energy corrections (see Section 3.3) is able to compensate for this.

The effect of the ENPT2 energy corrections is clearly illustrated by the errors for the uncorrected excitation energies (shown in orange in Figure 2). Here, a much more severe degradation in the quality of the excitation energies with decreasing pruning threshold value is observed, highlighting the importance of the ENPT2 energy corrections. For reference, we also show in Figure 3 a comparison of the RMSDs of the excitation energies as a function of α_p both with and without the application of the ENPT2 energy corrections. As may be expected, the RMSDs for the non-corrected excitation energies scale approximately linearly with α_p . Application of the ENPT2 energy corrections clearly breaks this relationship, particularly for smaller values of α_p .

Also shown in Figure 3 are the maximum errors as a function of the pruning threshold.

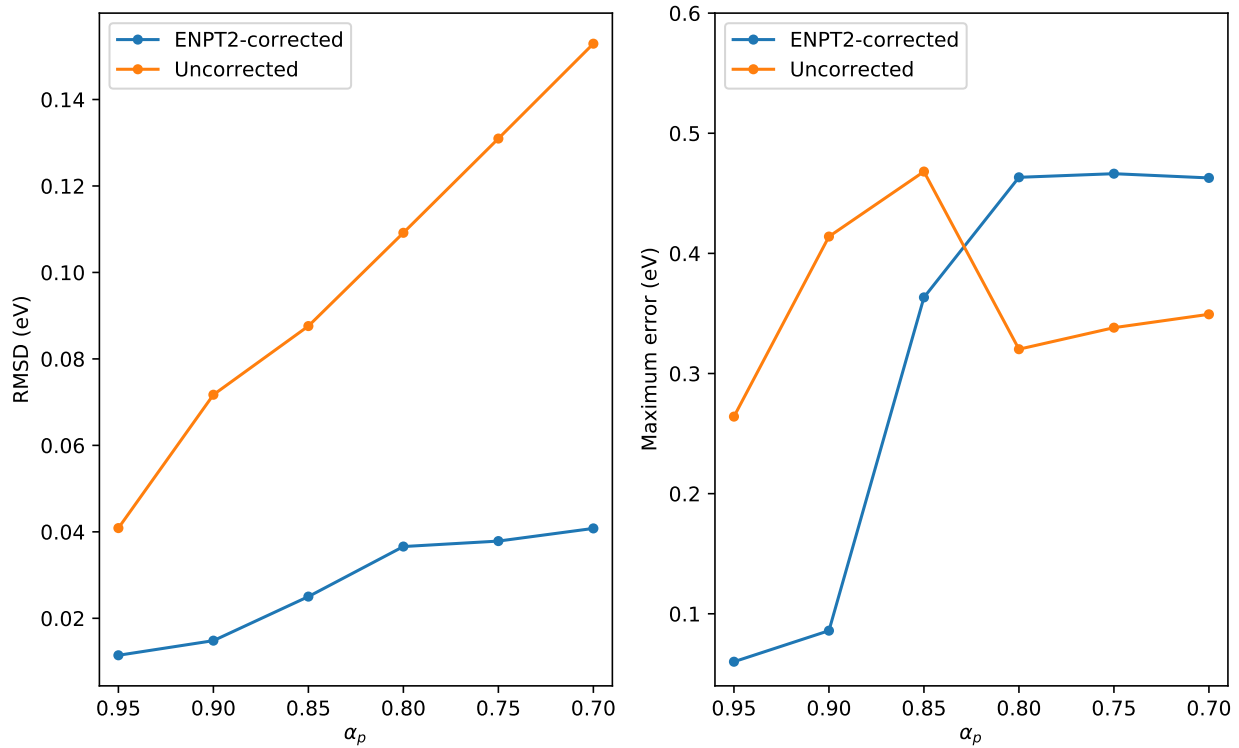


Figure 3: Comparison of RMSDs and maximum errors of excitation energies as a function of the pruning threshold α_p , both with and without the ENPT2 energy correction applied. All values correspond to an energy-based selection threshold of $\delta E_{sel} = 1.0 E_h$.

Here, the situation appears to be worse, with maximum errors of greater than 0.3 eV being seen for all values of $\alpha_p < 0.90$, both with and without the application of the ENPT2 energy corrections. In fact, the maximum errors for values of $\alpha_p < 0.85$ are larger for the ENPT2 energy corrected values than for the uncorrected ones. In most cases the largest errors in the ENPT2 energy-corrected values arise due to the extremal roots computed in the pruned and unpruned calculations corresponding to different states. This can usually be ameliorated by computing a handful of extra roots. However, in order to avoid this problem, it seems advisable to not use a pruning threshold α_p significantly below 0.90.

4.2 Reduction in size of the CSF basis

Having established the generally favorable errors introduced by the combination of configuration pruning and ENPT2 energy corrections, we now turn our attention to the computational gains afforded by the p-DFT/MRCI method. To do so, we consider the reduction of the CSF basis size as a function of the pruning threshold. Here, we consider only values of $\alpha_p = 0.95$ and 0.90, which, as discussed in Section 4.1, are found to consistently yield small maximum errors.

As a measure of the speedups resulting from the configuration pruning algorithm, we consider the CSF basis compression factor

$$\kappa(\alpha_p) = \frac{N_{CSF}(\alpha_p = 1)}{N_{CSF}(\alpha_p)}. \quad (14)$$

That is, the ratio of the number of CSFs without and with the application of configuration pruning as a function of the pruning threshold α_p . We note that the cost of a single DFT/MRCI Hamiltonian build scales empirically as $\mathcal{O}(N_{CSF}^m)$, $m \sim 1.3 - 1.5$. Thus, although the individual configuration selection inherent to the DFT/MRCI method precludes an exact scaling relationship, we may expect speedups of the order of $\kappa^m(\alpha_p)$, $m \sim 1.3 - 1.5$ to be afforded by the p-DFT/MRCI method.

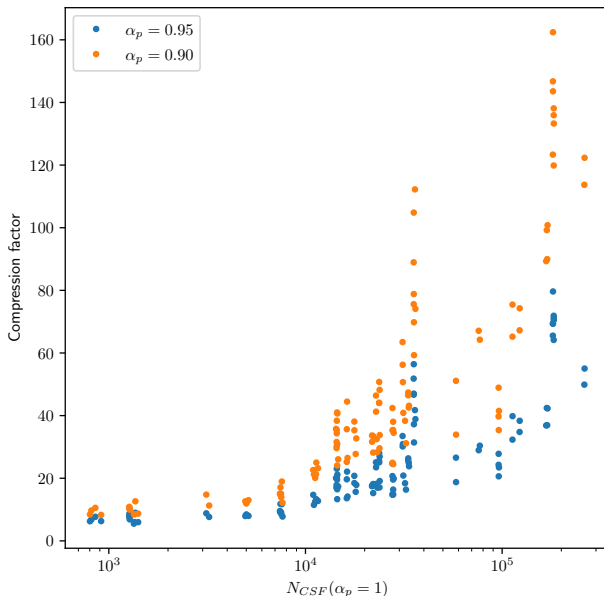


Figure 4: CSF basis compression factors as a function of the unpruned number of CSFs, $N_{CSF}(\alpha_p = 1)$, for pruning thresholds α_p of 0.95 and 0.90. All values correspond to an energy-based selection threshold of $\delta E_{sel} = 1.0 E_h$.

Shown in Figure 4 are the CSF basis compression factors as a function of the number of CSFs in the unpruned basis. For both $\alpha_p = 0.95$ and 0.90, there is a clear trend towards higher compression factors with increasing size of the unpruned CSF basis. That is, the computational savings introduced by configuration pruning are greatest for larger systems. For $\alpha_p = 0.95$, maximal compression factors in the range 60-80 are found. For $\alpha_p = 0.90$, this increases to around 100-160. Assuming a lower bound of $\mathcal{O}(N_{CSF}^{1.3})$ for the scaling of the cost of a DFT/MRCI Hamiltonian build, this translates into conservative speedup estimates of the order of 100-1000 \times . It is important to note that the largest molecule present in the test set (naphthalene) is still relatively small, and that, from the trends observed, we anticipate even greater gains upon increasing molecular size.

Finally, we note that the average CSF basis compression factor for $\alpha_p = 0.90$ is 1.8 times higher than for $\alpha_p = 0.95$. Considering the negligible increase in the error introduced by this change in pruning threshold, we recommend using a value of $\alpha_p = 0.90$ for an optimal balance of accuracy and computation effort.

4.3 Energy-based configuration selection

Separate from the configuration pruning algorithm presented here, there does exist another mechanism for reducing the size of the DFT/MRCI CSF basis. Namely, the reduction of the energy-based configuration selection threshold δE_{sel} (see Section 2). Indeed, all existing DFT/MRCI Hamiltonians have been separately parameterised for values of both $\delta E_{sel} = 1.0 E_h$ and $\delta E_{sel} = 0.8 E_h$. When the smaller of the two values, a significant reduction of the CSF basis does result. Thus, it is desirable to consider the errors and CSF basis reductions introduced by using $\delta E_{sel} = 0.8 E_h$, and to compare these with those afforded by the configuration pruning algorithm.

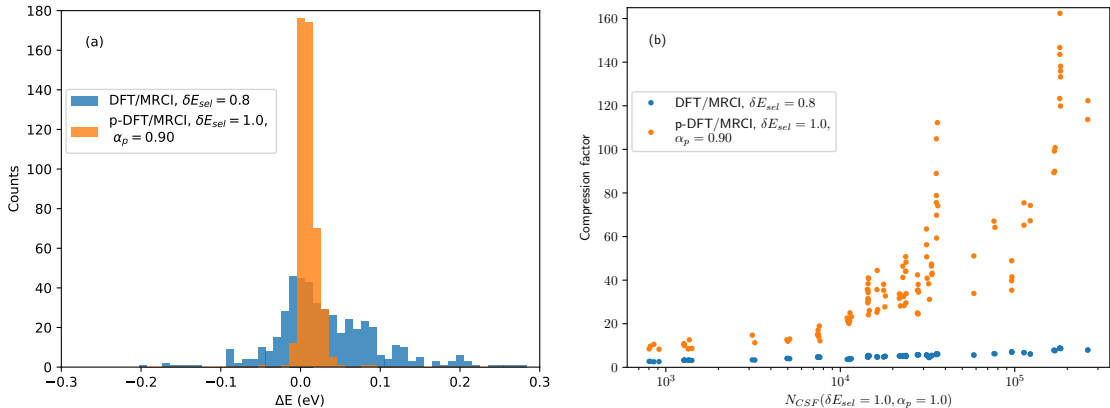


Figure 5: Comparison of: (a) excitation energy errors, and (b) CSF basis compression factors introduced decreasing energy-based selection threshold δE_{sel} (blue) and using configuration pruning (orange). All values are taken relative to the unpruned ($\alpha_p = 1.0$) calculations using an energy-based selection threshold of $\delta E_{sel} = 1.0 E_h$.

Shown in Figure 5 are both the errors in the excitation energies and the CSF basis compression factors introduced upon reduced the energy-based configuration selection threshold, δE_{sel} , from 1.0 to 0.8 E_h . For reference, the corresponding values resulting from p-DFT/MRCI calculations using selection thresholds $\delta E_{sel} = 1.0 E_h$ and $\alpha_p = 0.90$ are shown alongside. Reducing δE_{sel} from 1.0 to 0.8 E_h results in excitation energy errors with an RMSD 0.074 eV is found. This is to be compared to values of less than 0.015 eV for the p-DFT/MRCI results with $\alpha_p \leq 0.90$. Moreover, for the test set considered, there exist

no CSF basis compression factors greater than 10. This is to be compared with a maximum value of ~ 160 for the p-DFT/MRCI results. We thus conclude that the configuration pruning algorithm is to be favored over decreasing the energy-based configuration selection threshold, δE_{sel} , both in terms of accuracy and computational effort.

4.4 Computational costs

4.4.1 CPU times

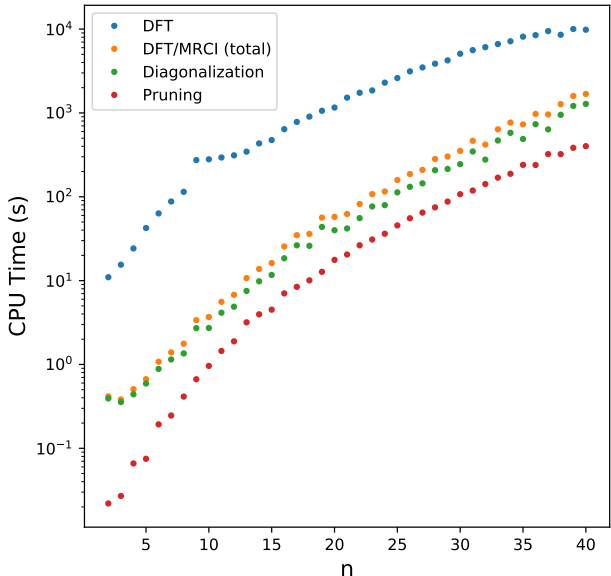


Figure 6: Timings for the main steps involved in a pruned DFT/MRCI calculation of the first excited state of each symmetry for a series of linear alkanes C_nH_{2n+2} . The def2-SVP basis set was used along with a pruning threshold $\alpha_p = 0.90$ and an energy-based selection threshold of $\delta E_{sel} = 1.0 E_h$. All calculations were performed on a single Intel Xeon E5-2660 v4 CPU core.

We end by considering the computational costs p-DFT/MRCI calculations for a representative example: the series of linear alkanes C_nH_{n+2} for n up to 40. In these calculations, the first excited state of each symmetry was computed (a total of five roots, including the ground state). The def2-SVP basis and def2-SVP-jkfit auxiliary basis were used along with a pruning threshold of $\alpha_p = 0.90$. Shown in Figure 6 are the calculation timings obtained using single

Intel Xeon E5-2660 v4 CPU core. Here, the timings are broken down into the three main steps: the preceding DFT calculation, and the configuration pruning and the DFT/MRCI Hamiltonian diagonalization steps. Although the absolute timings are hardware- and implementation dependent, some useful conclusions may still be drawn. First, it is evident that the pruning step introduces very little overhead, with the total p-DFT/MRCI calculation being dominated by the Hamiltonian diagonalization step. Second, for all members of the series C_nH_{n+2} up to $n = 40$, the preceding DFT calculation (performed using the PySCF package^{35,36}) is significantly more expensive than the subsequent p-DFT/MRCI calculation. The ratio of the two timings does decrease with increasing system size. However, even for the largest system size considered ($C_{40}H_{82}$, 322 electrons, 970 MOs), the p-DFT/MRCI calculation is still around six times quicker than the prerequisite DFT calculation. Important to note here is that this performance was attained using a relatively inefficient pilot implementation of the DFT/MRCI method, and this ratio will only increase with code optimization and algorithmic development.

4.4.2 Memory requirements

Although the use of configuration pruning helps to alleviate the Hamiltonian diagonalization bottleneck, the p-DFT/MRCI method is currently practically limited to around 1500-2000 correlated MOs. The reason for this is a steeply increasing memory cost associated with the storage of two-electron integrals.

Common to all selected CI methods, DFT/MRCI suffers from the property that σ -vector (i.e., Hamiltonian matrix-vector product) calculations cannot efficiently be made integral-driven. Instead, a configuration-driven algorithm is used, in which ‘arbitrary’ sets of two-electron integrals are required to be accessed on an element-by-element basis. In turn, this necessitates the in-core storage of the two-electron integrals, which in practice are decomposed using density fitting (DF) to reduce storage costs. Even with the use of DF, however, the memory cost still scales as $\mathcal{O}(N_{MO}^3)$, resulting in tremendous costs for $N_{MO} \gtrsim 2000$. By

way of example, extending the linear alkanes example to $n=100$ ($C_{100}H_{202}$) would require 483 GB RAM for the storage of the two-electron integrals.

Clearly, in order to extend the p-DFT/MRCI method to larger systems, a different route must be perused. One potential strategy would be to use a different decomposition of the two-electron integral tensor. A promising candidate is the tensor hypercontraction (THC) method of Martínez *et al.*⁴⁶⁻⁴⁸ Using THC in place of DF, the integral storage cost would be decrease to $\mathcal{O}(N_{MO}^2)$, significantly increasing the size of system amenable to application of the p-DFT/MRCI method.

5 Conclusions

We have presented an approach for the removal of deadwood configurations from DFT/MRCI calculations. The proposed algorithm, termed p-DFT/MRCI, is based on a computationally cheap pruning step, utilizing Epstein-Nesbet perturbation theory to estimate the contribution of each individual configuration to the eigenstates of interest. By combining this pruning scheme with a simple, state-specific energy correction to account for the pruned configurations, a reduction of the CSF basis size by up to two orders of magnitude can be achieved while introducing negligible errors.

A pre-requisite of the configuration pruning algorithm is that an initial reference space with good support of the desired eigenstates be used. To address this, an automated initial reference space generation algorithm was devised and implemented, based on an approximate preliminary DFT/CIS calculation. The result is a black box method controlled by a single pruning threshold parameter, α_p .

From the test set of small-to-medium sized molecules considered here, it is apparent that the proportion of configurations removed by the pruning scheme increases significantly with the system size. Accordingly, we expect that the already impressive CSF basis reduction factors reported here will only increase when larger molecules are considered.

It remains to note that, although the use configuration pruning alleviates the Hamiltonian diagonalization bottleneck to a significant degree, the p-DFT/MRCI method is still limited by an integral storage cost scaling as $\mathcal{O}(N_{MO}^3)$ in its current DF-based implementation. This should be alleviated by adopting a lower scaling decomposition of the two-electron integral tensor. The use of THC decomposition appears highly promising in this regard and will be the subject of future work, laying the way for the application of p-DFT/MRCI to systems of unprecedented size.

References

- (1) Grimme, S.; Waletzke, M. A combination of Kohn–Sham density functional theory and multi-reference configuration interaction methods. *The Journal of Chemical Physics* **1999**, *111*, 5645–5655.
- (2) Lyskov, I.; Kleinschmidt, M.; Marian, C. M. Redesign of the DFT/MRCI Hamiltonian. *The Journal of Chemical Physics* **2016**, *144*, 034104.
- (3) Heil, A.; Marian, C. M. DFT/MRCI Hamiltonian for odd and even numbers of electrons. *The Journal of Chemical Physics* **2017**, *147*, 194104.
- (4) Heil, A.; Kleinschmidt, M.; Marian, C. M. On the performance of DFT/MRCI Hamiltonians for electronic excitations in transition metal complexes: The role of the damping function. *The Journal of Chemical Physics* **2018**, *149*, 164106.
- (5) Seidu, I.; Neville, S. P.; Kleinschmidt, M.; Heil, A.; Marian, C. M.; Schuurman, M. S. The simulation of X-ray absorption spectra from ground and excited electronic states using core-valence separated DFT/MRCI. *The Journal of Chemical Physics* **2019**, *151*, 144104.
- (6) Kleinschmidt, M.; Marian, C. M. Efficient generation of matrix elements for one-electron

- spin-orbit operators. *Chemical Physics* **2005**, *311*, 71–79, Relativistic Effects in Heavy-Element Chemistry and Physics. In Memoriam Bernd A. Hess (1954–2004).
- (7) Kleinschmidt, M.; Tatchen, J.; Marian, C. M. SPOCK.CI: A multireference spin-orbit configuration interaction method for large molecules. *The Journal of Chemical Physics* **2006**, *124*, 124101.
- (8) Neville, S. P.; Seidu, I.; Schuurman, M. S. Propagative block diagonalization diabaticization of DFT/MRCI electronic states. *The Journal of Chemical Physics* **2020**, *152*, 114110.
- (9) Marian, C. M.; Heil, A.; Kleinschmidt, M. The DFT/MRCI method. *WIREs Computational Molecular Science* **2019**, *9*, e1394.
- (10) Bender, C. F.; Davidson, E. R. Studies in Configuration Interaction: The First-Row Diatomic Hydrides. *Phys. Rev.* **1969**, *183*, 23–30.
- (11) Whitten, J. L.; Hackmeyer, M. Configuration Interaction Studies of Ground and Excited States of Polyatomic Molecules. I. The CI Formulation and Studies of Formaldehyde. *The Journal of Chemical Physics* **1969**, *51*, 5584–5596.
- (12) Hackmeyer, M.; Whitten, J. L. Configuration Interaction Studies of Ground and Excited States of Polyatomic Molecules II. The Electronic States and Spectrum of Pyrazine. *The Journal of Chemical Physics* **1971**, *54*, 3739–3750.
- (13) Buenker, R. J.; Peyerimhoff, S. D. Individualized configuration selection in CI calculations with subsequent energy extrapolation. *Theoret. Chim. Acta* **1974**, *35*, 33.
- (14) Buenker, R. J.; Peyerimhoff, S. D. Energy extrapolation in CI calculations. *Theoret. Chim. Acta* **1975**, *39*, 217.
- (15) Buenker, R. J.; Peyerimhoff, S. D.; Butscher, W. Applicability of the multi-reference

- double-excitation CI (MRD-CI) method to the calculation of electronic wavefunctions and comparison with related techniques. *Molecular Physics* **1978**, *35*, 771–791.
- (16) Huron, B.; Malrieu, J. P.; Rancurel, P. Iterative perturbation calculations of ground and excited state energies from multiconfigurational zeroth-order wavefunctions. *The Journal of Chemical Physics* **1973**, *58*, 5745–5759.
- (17) Garniron, Y. et al. Quantum Package 2.0: An Open-Source Determinant-Driven Suite of Programs. *Journal of Chemical Theory and Computation* **2019**, *15*, 3591–3609, PMID: 31082265.
- (18) Loos, P.-F.; Damour, Y.; Scemama, A. The performance of CIPSI on the ground state electronic energy of benzene. *The Journal of Chemical Physics* **2020**, *153*, 176101.
- (19) Garniron, Y. Développement et implémentation parallèle de méthodes d’interaction de configurations sélectionnées. Ph.D. thesis, 2018; Thèse de doctorat dirigée par Scemama, Anthony Physico-Chimie Théorique Toulouse 3 2018.
- (20) Holmes, A. A.; Tubman, N. M.; Umrigar, C. J. Heat-Bath Configuration Interaction: An Efficient Selected Configuration Interaction Algorithm Inspired by Heat-Bath Sampling. *Journal of Chemical Theory and Computation* **2016**, *12*, 3674–3680, PMID: 27428771.
- (21) Sharma, S.; Holmes, A. A.; Jeanmairet, G.; Alavi, A.; Umrigar, C. J. Semistochastic Heat-Bath Configuration Interaction Method: Selected Configuration Interaction with Semistochastic Perturbation Theory. *Journal of Chemical Theory and Computation* **2017**, *13*, 1595–1604, PMID: 28263594.
- (22) Holmes, A. A.; Umrigar, C. J.; Sharma, S. Excited states using semistochastic heat-bath configuration interaction. *The Journal of Chemical Physics* **2017**, *147*, 164111.

- (23) Li, J.; Otten, M.; Holmes, A. A.; Sharma, S.; Umrigar, C. J. Fast semistochastic heat-bath configuration interaction. *The Journal of Chemical Physics* **2018**, *149*, 214110.
- (24) Tubman, N. M.; Lee, J.; Takeshita, T. Y.; Head-Gordon, M.; Whaley, K. B. A deterministic alternative to the full configuration interaction quantum Monte Carlo method. *The Journal of Chemical Physics* **2016**, *145*, 044112.
- (25) Tubman, N. M.; Freeman, C. D.; Levine, D. S.; Hait, D.; Head-Gordon, M.; Whaley, K. B. Modern Approaches to Exact Diagonalization and Selected Configuration Interaction with the Adaptive Sampling CI Method. *Journal of Chemical Theory and Computation* **2020**, *16*, 2139–2159, PMID: 32159951.
- (26) Schriber, J. B.; Evangelista, F. A. Communication: An adaptive configuration interaction approach for strongly correlated electrons with tunable accuracy. *The Journal of Chemical Physics* **2016**, *144*, 161106.
- (27) Schriber, J. B.; Evangelista, F. A. Adaptive Configuration Interaction for Computing Challenging Electronic Excited States with Tunable Accuracy. *Journal of Chemical Theory and Computation* **2017**, *13*, 5354–5366, PMID: 28892621.
- (28) Zhang, N.; Liu, W.; Hoffmann, M. R. Iterative Configuration Interaction with Selection. *Journal of Chemical Theory and Computation* **2020**, *16*, 2296–2316, PMID: 32069046.
- (29) Zhang, N.; Liu, W.; Hoffmann, M. R. Further Development of iCIPT2 for Strongly Correlated Electrons. *Journal of Chemical Theory and Computation* **2021**, *17*, 949–964, PMID: 33410692.
- (30) Chilkuri, V. G.; Neese, F. Comparison of many-particle representations for selected-CI I: A tree based approach. *Journal of Computational Chemistry* **2021**, *42*, 982–1005.
- (31) Chilkuri, V. G.; Neese, F. Comparison of Many-Particle Representations for Selected

- Configuration Interaction: II. Numerical Benchmark Calculations. *Journal of Chemical Theory and Computation* **2021**, *17*, 2868–2885, PMID: 33886300.
- (32) Olsen, J.; Roos, B. O.; Jørgensen, P.; Jensen, H. J. A. Determinant based configuration interaction algorithms for complete and restricted configuration interaction spaces. *The Journal of Chemical Physics* **1988**, *89*, 2185–2192.
- (33) Grimme, S. Density functional calculations with configuration interaction for the excited states of molecules. *Chemical Physics Letters* **1996**, *259*, 128–137.
- (34) Neville, S. P.; Schuurman, M. S. GRaCI: General Reference Configuration Interaction. 2021; <https://github.com/schuurman-group/graci.git>.
- (35) Sun, Q.; Berkelbach, T. C.; Blunt, N. S.; Booth, G. H.; Guo, S.; Li, Z.; Liu, J.; McClain, J. D.; Sayfutyarova, E. R.; Sharma, S.; Wouters, S.; Chan, G. K.-L. PySCF: the Python-based simulations of chemistry framework. *WIREs Computational Molecular Science* **2018**, *8*, e1340.
- (36) Sun, Q. et al. Recent developments in the PySCF program package. *The Journal of Chemical Physics* **2020**, *153*, 024109.
- (37) Whitten, J. L. Coulombic potential energy integrals and approximations. *The Journal of Chemical Physics* **1973**, *58*, 4496–4501.
- (38) Feyereisen, M.; Fitzgerald, G.; Komornicki, A. Use of approximate integrals in ab initio theory. An application in MP2 energy calculations. *Chemical Physics Letters* **1993**, *208*, 359–363.
- (39) Vahtras, O.; Almlöf, J.; Feyereisen, M. Integral approximations for LCAO-SCF calculations. *Chemical Physics Letters* **1993**, *213*, 514–518.
- (40) Wetmore, R. W.; Segal, G. A. Efficient generation of configuration interaction matrix elements. *Chemical Physics Letters* **1975**, *36*, 478–483.

- (41) Segal, G. A.; Wetmore, R. W.; Wolf, K. Efficient methods for configuration interaction calculations. *Chemical Physics* **1978**, *30*, 269–297.
- (42) Hanrath, M.; Engels, B. New algorithms for an individually selecting MR-CI program. *Chemical Physics* **1997**, *225*, 197–202.
- (43) Scemama, A.; Giner, E. An efficient implementation of Slater-Condon rules. 2013.
- (44) Schreiber, M.; Silva-Junior, M. R.; Sauer, S. P. A.; Thiel, W. Benchmarks for electronically excited states: CASPT2, CC2, CCSD, and CC3. *The Journal of Chemical Physics* **2008**, *128*, 134110.
- (45) Dunning, T. H. Gaussian basis sets for use in correlated molecular calculations. I. The atoms boron through neon and hydrogen. *The Journal of Chemical Physics* **1989**, *90*, 1007–1023.
- (46) Hohenstein, E. G.; Parrish, R. M.; Martínez, T. J. Tensor hypercontraction density fitting. I. Quartic scaling second- and third-order Møller-Plesset perturbation theory. *The Journal of Chemical Physics* **2012**, *137*, 044103.
- (47) Parrish, R. M.; Hohenstein, E. G.; Martínez, T. J.; Sherrill, C. D. Tensor hypercontraction. II. Least-squares renormalization. *The Journal of Chemical Physics* **2012**, *137*, 224106.
- (48) Hohenstein, E. G.; Parrish, R. M.; Sherrill, C. D.; Martínez, T. J. Communication: Tensor hypercontraction. III. Least-squares tensor hypercontraction for the determination of correlated wavefunctions. *The Journal of Chemical Physics* **2012**, *137*, 221101.